APPLICATION OF FRACTAL MODELING BASED ON REMOTE SENSING DATA FOR DETECTING IRON MINERALIZATION IN DEHSHIR–BAFT FAULT, WEST OF CENTRAL IRAN

APLICAÇÃO DE MODELO FRACTAL BASEADO EM DADOS DE SENSORIAMENTO REMOTO PARA DETECTAR MINERAÇÕES DE FERRO NA FALHA DEHSHIR-BAFT, NA REGIÃO OESTE DO IRÃ CENTRAL

Faezeh Ahmadi[1]

Mohammad Reza Jafari[2]

Ahmad Adib*[3]

Hamid Hrati[4]

Mohammad Ali Arian[5]

ABSTRACT

Part of Dehshir–Baft Fault is located on the 1:100000 Sarvbala geological sheet west of Yazd Province in Iran on the Urmia–Dokhtar magmatic–mineralization zone. Regions with iron mineralization potential on this sheet were detected by identifying alterations and fault trends by processing ASTER satellite images. Images were processed using the false color composite (FCC), Crosta, LS-Fit, and spectral angle mapper (SAM) methods to identify iron oxide, argillic, propylitic, and phyllic alterations. To find out the role of faults and lineaments in mineralization, the general faulting trend on this sheet was extracted by relief shading on the digital elevation model (DEM), and the fault zones were examined through field operations. Regions with high iron potential were identified by integrating the fault layers, alterations, and mineralization-related geological units in ArcGIS. The identified regions were then validated through field operations. The relationship between the distance of iron oxide alterations obtained from the LS-Fit method with the main fault was evaluated by the fractal method. The results showed the location and more significant relationship of iron potential with faults in the south and southwest of Sarvbala sheet than other regions.

Keywords: Sarvbala; Alteration; ASTER; LS-Fit; SAM

RESUMO

[1]Ph.D. Student, Department of Geology, North Tehran Branch, Islamic Azad University, Tehran, Iran. fff_geo@yahoo.com ORCID: https://orcid.org/0000-0002-4195-2839

[2]Assistant Professor, Department of Geology, North Tehran Branch, Islamic Azad University, Tehran, Iran. mr.jafari_1348@yahoo.com ORCID: https://orcid.org/0000-0003-2815-2009

[3]Department of Petroleum Engineering, South Tehran Branch, Islamic Azad University, Tehran, Iran. *Corresponding author. adib@azad.ac.ir ORCID: https://orcid.org/0000-0002-5432-4612

[4]Department of Geology, Payame Noor University, Tehran, Iran hamid.harati437@yahoo.com ORCID: https://orcid.org/0000-0003-0543-5233

[5]Department of Geology, Faculty of Sciences, North Tehran Branch, Islamic Azad University, Tehran, Iran. m-arian@iau-tnb.ac.ir ORCID: https://orcid.org/0000-0001-8193-0274

Revista Geoaraguaia – **ISSN: 2236-9716** – V.10 n. Especial Geologia e Pedologia. Dez-2020

130

Parte da falha de Dehshir – Baft está localizada na folha geológica Sarvbala 1: 100.000 a oeste da província de Yazd, no Irã, na zona de mineração magmática Urmia – Dokhtar. A pesquisa conduzida buscou indetificar regiões com potencial de mineração de ferro nesta folha a partir da detecção e identificação de alterações e tendências de falha pelo processamento de imagens de satélite do instrumento ASTER. As imagens foram processadas usando os métodos de composição falsa cor (FCC), Crosta, LS-Fit e mapemaneto de ângulo espectral (SAM) para identificar alterações de óxido de ferro, argílico, propilítico e fílico na área. Para descobrir o papel das falhas e lineamentos na mineração, a tendência geral de falhas nesta folha foram obtidas com a elaboração do sombreamento do relevo no Modelo Digital de Elevação (DEM), e as zonas de falha foram examinadas por meio de verificações de campo. Regiões com alto potencial de ferro foram identificadas através da integração das camadas de falha, alterações e unidades geológicas relacionadas à mineração com o uso do programa ArcGIS. As regiões identificadas foram então validadas *in loco*. A relação entre a distância das alterações do óxido de ferro obtida pelo método LS-Fit com a falha principal foi avaliada pelo método fractal. Os resultados mostraram a localização e a relação mais significativa do potencial de ferro com as falhas no sul e sudoeste da folha do mapa geológico de Sarvbala do que em outras regiões.

Palavras-Chave: Sarvbala; Alteração geológica; ASTER; LS-Fit; Mapeamento de ângulo espectral

INTRODUCTION

The 1:100000 Sarvbala, Dehshir and Khezrabad sheets are located in the west of Central Iran, west of Yazd Province, and south of the 1:250000 Naeen sheet along the Urmia–Dokhtar metallogenic belt. Multiple iron, copper, gold, uranium, nickel, vanadium, molybdenum, and rhenium mineralizations are found along this belt (Shahabpour, 1994, Afzal *et al.*, 2012, Aghazadeh *et al.*, 2015, Abdoli Sereshgi *et al.*, 2019, Daya 2019). The presence of intrusive masses and big Soork and Almason iron ore mines respectively in the north and south of Dehshir Fault (Adib, 2011) in the Sarvbala and Dehshir sheets is indicative of the high potential of these regions (Yazd Rolling Mill Co., 1:1000 geological map of Soork mine blocks, 1392). A major part of these sheets in the main Dehshir–Baft Fault exists as an active earthquake-generating (seismogenic) fault (Adib, Mehrnahad, 1999). The north-northwest (NNW)-south-southeast (SSE) Dehshir Fault intersects part of the Sanandaj–Sirjan, Urmia–Dokhtar magmatic arc, and Central Iran structural zones, and is considered the western boundary of the right-slip northern-southern faults in Central Iran and the east of

Revista Geoaraguaia – **ISSN: 2236-9716** – V.10 n. Especial Geologia e Pedologia. Dez-2020

131

Iran. This fault is of great importance in terms of color blending expansion (Ahmadi and Sheykhi., 2019, Shafaii *et al.*, 2010).

The study of multispectral images is very important and useful for the exploration and identification of hydrothermal altered areas. Also, remote sensing (i.e., ASTER) images, which have suitable spectral and spatial resolutions, are used in the effective recognition of hydrothermal alteration and structures (Aramesh Asl *et al.* 2015, Novruzov *et al.*, 2019).

The ideas on the relationship of mineralization and geological structures demonstrate the key role of these structures in the formation of minerals (Craw and Campbell, 2004; Drew, 2006; Wang *et al.*, 2012). Understanding this structural situation can be an exploration key, and satellite and airborne geophysical data are also useful tools for determination of alteration zones. This relationship can be more effectively determined with the help of fractal geometry methods (Ulrich *et al.*, 2001). The geochemical distribution and dispersion of elements and mineralization is a function of geological, igneous, sedimentary, structural, tectonic, and metamorphic processes. These processes have self-similarity features with fractal and multi-fractal properties (Yousefifar, 2011, Ghavami-Rajabi, 2007; Khalajmasoumi *et al.*, 2016; Afzal *et al.*, 2017, Yazdi *et al.*, 2019 a and b, Yasrebi and Hezarkhani., 2019). The literature (Bolviken *et al.*, 1992; Cheng *et al.*, 1994; Agterberg *et al.*, 1996) reveals a fractal correlation between the grade and concentration of elements and their geometrical characteristics of geochemical dispersion. Nouri *et al.* (2013) found a positive correlation between mineralization and structures in Tarom (Zanjan, Iran) using the concentration–distance major fault (C–DMF) fractal models.

The spectral angle mapper (SAM) identifies alteration-related minerals with high precision and eliminates most disadvantages of traditional old methods (Feizi and Mansouri, 2013). This study aims at identifying alterations and spectral behavior of alteration-related minerals, faults, and lineaments through processing satellite images and integrating data obtained in ArcGIS. Using these tools, regions with high iron mineralization potential are

Revista Geoaraguaia – **ISSN: 2236-9716** – V.10 n. Especial Geologia e Pedologia. Dez-2020

132

identified, and the approximate distance of iron oxide alterations from Dehshir–Baft Fault in Sarvbala sheet is determined.

GEOLOGY OF THE STUDY AREA

Sarvbala geological sheet is located between the longitudes 53° and 53° 30' and the latitudes 32° and 32° 30' in the west of Yazd Province in Iran. The lithological units in the study area can be classified into three categories: (1) pre-Eocene sedimentary and igneous rocks with severe folding and faulting in the northeast corner, (2) Tertiary volcanic sedimentary rocks with mild folding in the western part and (3) a narrow strip of ophiolite complexes extended from the northwest to the southeast (Amidi, Nabavi, 1980). The major intrusive volcanic rocks mainly concentrated in the south of the sheet are aplitic granite, granite, granodiorite, and diorite (Amidi, Nabavi, 1980). Volcanic rocks include rhyodacite in the southeast and andesite basalts and trachyandesite in the center towards the west of this sheet. There are several abandoned lead and zinc mines in the northwest of the sheet towards Haftar (Amidi, Nabavi, 1980). Soork iron ore mine is the main deposit in Sarvbala sheet that its genesis can be related to the main Dehshir–Baft Fault. Multiple alterations are also observed around this fault (Zare, 1995) (Figures 1 and 2).
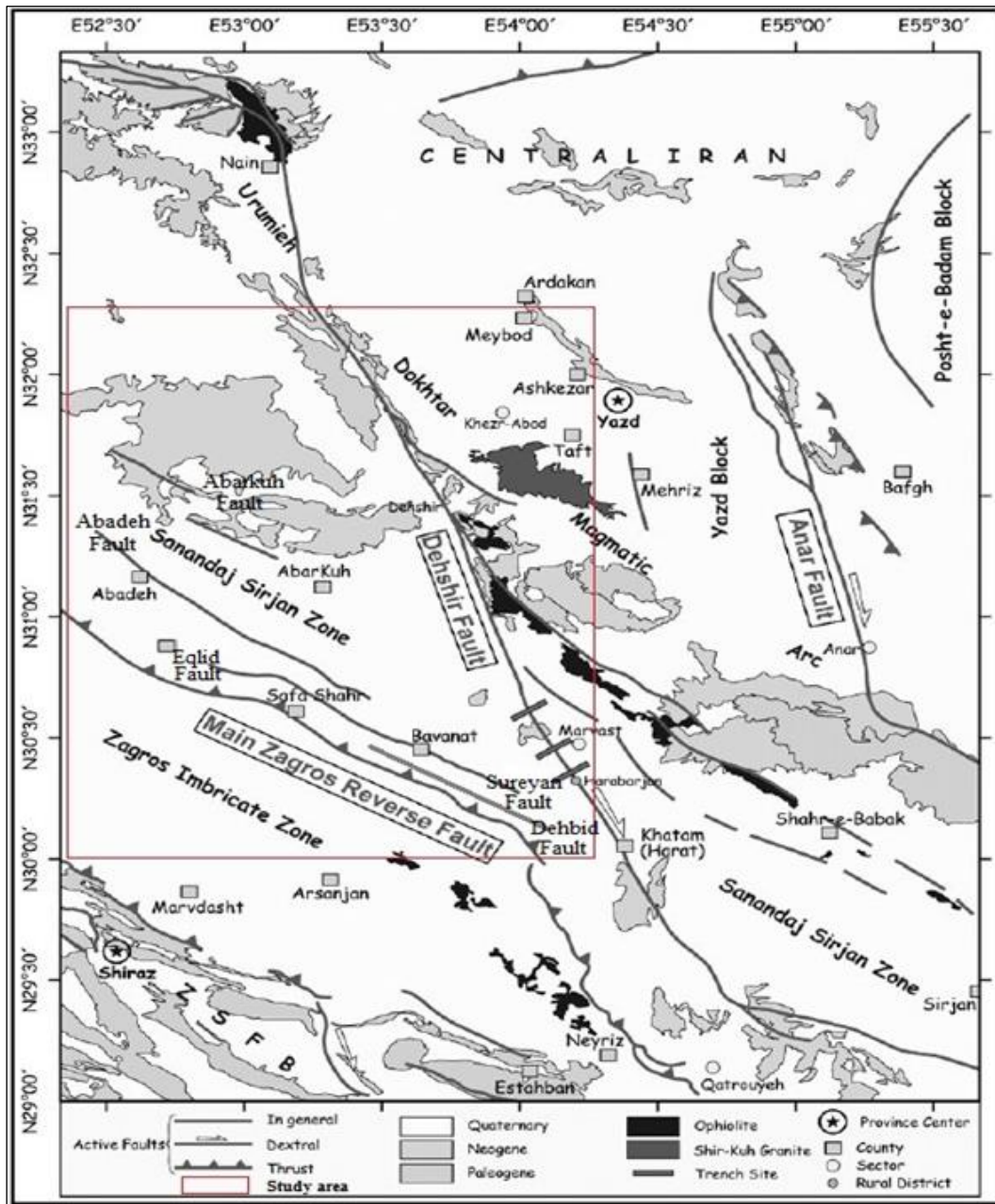
Revista Geoaraguaia – **ISSN: 2236-9716** – V.10 n. Especial Geologia e Pedologia. Dez-2020

133

Figure 1. Structural zones for the Dehshir Fault system and its surrounding zones.
Source: Modified after Hessami *et al.* (2003); Meyer *et al.* (2006); Meyer and Le Dortz (2007).
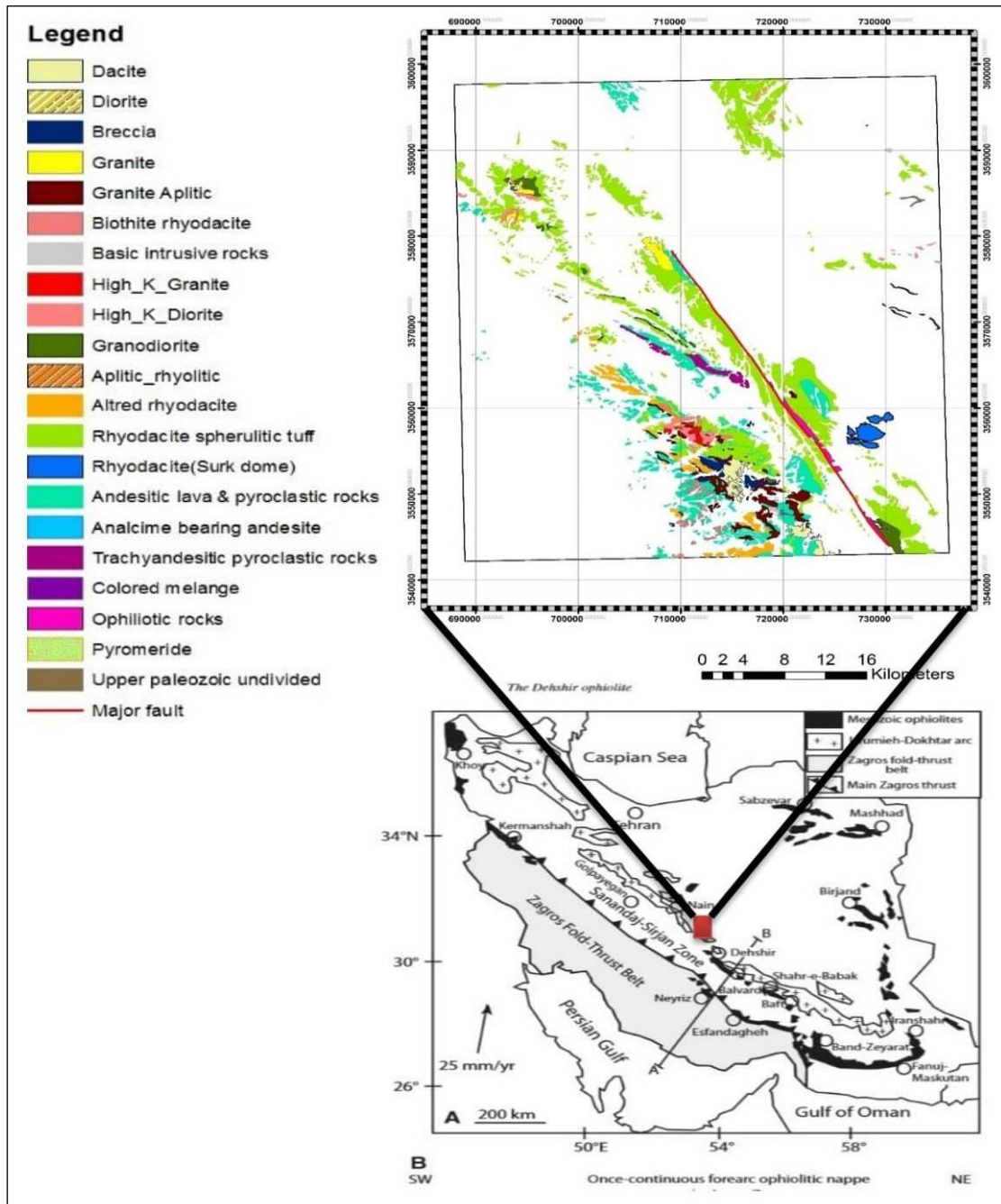
Revista Geoaraguaia – **ISSN: 2236-9716** – V.10 n. Especial Geologia e Pedologia. Dez-2020

134

Figure 2. The location of the sheet under study in the geological map of Iran and the 1:100000 map of the study area.
Source: Shafaii *et al.* (2010); Amidi, Nabavi (1980).

MATERIALS AND METHODS

The C-A fractal model has been proposed by Cheng *et al.* (1994) and applied for identification of geochemical and geophysical anomalies from background (Agterberg, 1996;

Revista Geoaraguaia – **ISSN: 2236-9716** – V.10 n. Especial Geologia e Pedologia. Dez-2020

135

Goncalves *et al.*, 1998; Sim *et al.*, 1999; Cheng, 1999; 2000; Afzal *et al.*, 2010; Hassanpour and Afzal, 2011; Zuo, 2011; Mohammadi *et al.*, 2013, Yazdi *et al.*, 2017, Nazarpour., 2018, Nazemi *et al.*, 2019, Zadmehr *et al.*, 2019).

The concentration-area (C-A) model serves to demonstrate the relationship correlated between the obtained results with the geological, geochemical, geophysical and remote sensing information. Its most useful features are the simple implementation and the ability to compute quantitative anomalous thresholds (Cheng *et al.*, 1994; Goncalves *et al.*, 2001; Cheng and Li, 2002). Cheng *et al.* (1994) proposed the Concentration–Area (C–A) method for separating geochemical alteration.

The Multispectral images method is a valuable technique of mapping lithology, mineralogy and exploration of anomalous area (Sabins, 1999; Mars and Rowan, 2006; Zhang *et al.*, 2007; Gabr *et al.*, 2010). Multispectral satellite images datasets that release data in varied diversities of electromagnetic range help investigator to recognize minerals. Every mineral has particular chemical composition and crystal structure with particular absorption and reflection variety in electromagnetic spectrum. Image analysis and processing methods be able to deduce the satellite images spectral such as Spectral Feature Fitting (SFF), Principal Components Analysis (PCA), Band Ratio (BR), Spectral Angle Mapper (SAM), Minimum Noise Fraction (MNF) and Least Squares Fitting method (LS-Fit) techniques. Many studies have been conducted on the exploration of minerals using satellite imagery. Mahanta and Maiti (2018), Ahmadirouhani *et al.*, (2018) and Noori *et al.*, (2019) used ASTER data to detect altered minerals from non-altered minerals.

Satellite data should be preprocessed using radiometric and geometric techniques. The Log Residuals method was used for radiometric correction. This method has been designed to eliminate solar radiation, atmospheric scattering, and topographic and Albedo effects based on the reflection of satellite images (Feizi and Mansouri, 2012). This transfer produces false reflection images which can be useful for terrain analysis and mineral

Revista Geoaraguaia – **ISSN: 2236-9716** – V.10 n. Especial Geologia e Pedologia. Dez-2020

136

applications. The software Envi5.1 was employed for this purpose, and a total of nine bands were used in the ASTER images.

FALSE COLOR COMPOSITE (FCC)

Various geological phenomena can be effectively identified by displaying image data as color data (Feizi and Mansouri, 2013). According to the USGS curves resampled by ASTER bands (Figure 3), minerals containing Al–OH bonds such as kaolinite, montmorillonite, illite, and muscovite (characteristic minerals in the argillic and phyllic alterations) with the maximum reflection in the band 4 of the SWIR region. The minerals containing Mg–OH bonds such as chlorite and epidote (characteristic minerals in the propylitic alteration) show a high absorption in the band 8 of the SWIR spectral region of ASTER. Therefore, in the RGB (4, 6, 8) false color composite (FCC) of the SWIR region, the phyllic and argillic alterations are observed in red to pink and the propylitic alteration in green, and lime-containing zones are observed in yellow (Figure 4).
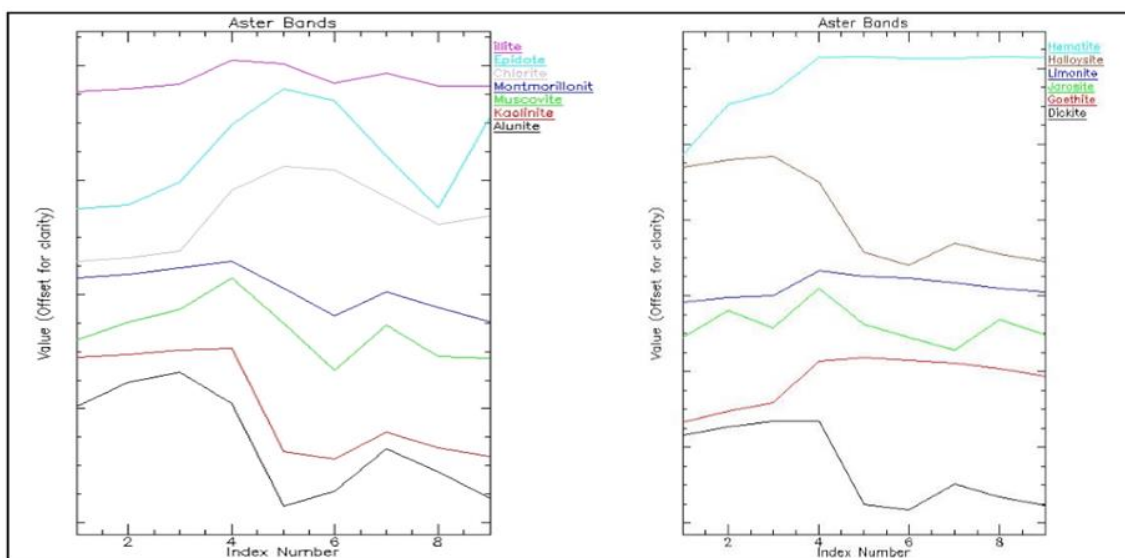

Figure 3. The spectral behavior of the characteristic minerals in the studied alterations from the USGS spectral library in Envi5.
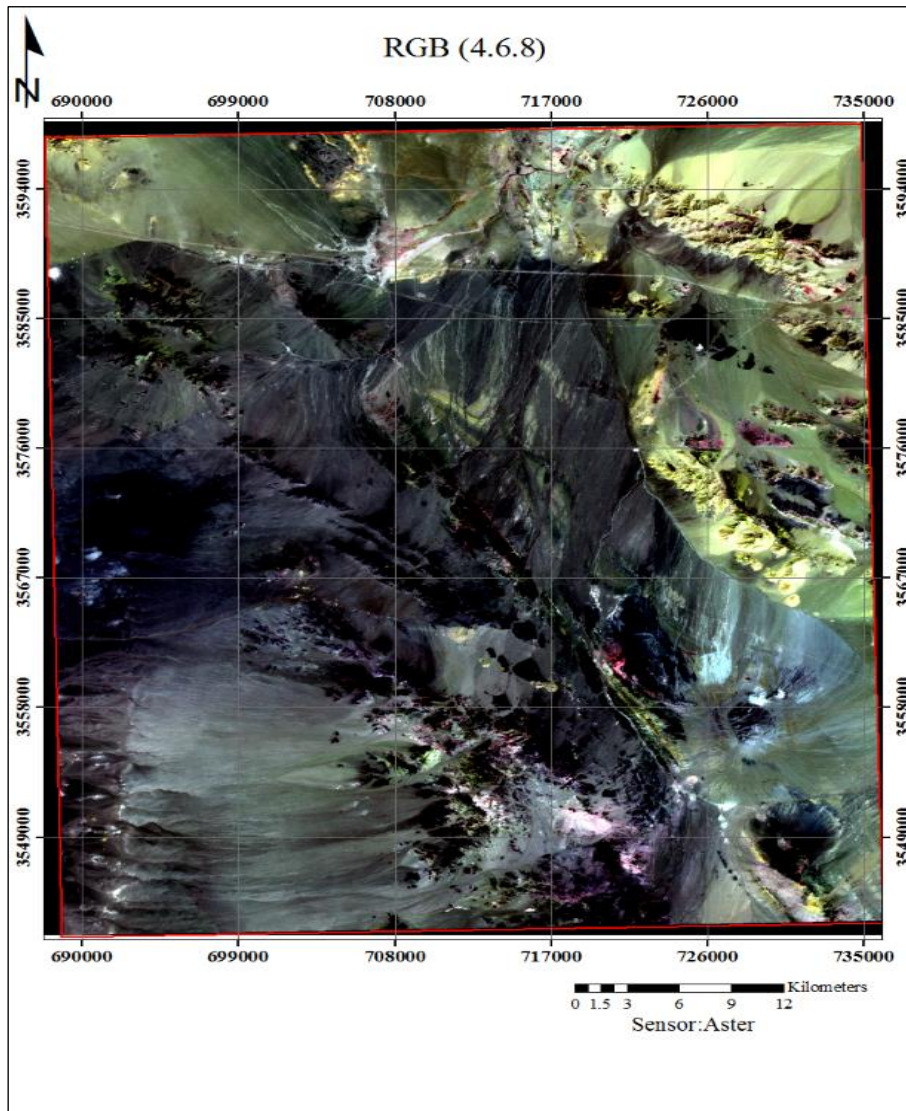Source: Feizi and Mansouri (2013).

Revista Geoaraguaia – **ISSN: 2236-9716** – V.10 n. Especial Geologia e Pedologia. Dez-2020

137

Figure 4. The sattelite image of the study area with the RGB (4, 6, 8) band, the argillic and phyllic alterations in pink, the propylitic alteration in green and the lime-containing zones in yellow. Source: Based on ASTER data (2020).

MAIN COMPONENT ANALYSIS ON ASTER IMAGES

The analysis of selected main components (Crosta) is perfromed to reduce data volume and repeating information or interfering phenomena such as topographic effects, solar radiation angel, and shadow. This involves decomposition of eigenvalues of the covariance matrix or the matrix of correlation coefficients (Toosi, 2015). The analysis of main components is in fact a orthogonal linear transoformation that transfers data to the new coordinate system and can be used to reduce data dimensions. Only cetrain bands containing

Revista Geoaraguaia – **ISSN: 2236-9716** – V.10 n. Especial Geologia e Pedologia. Dez-2020

138

useful information are used in the Crosta method, and other bands are neglected to prevent errors []. Given the characteristic minerals in the studied alterations, PC(1,2,3,4), PC(1,5,7,9), PC(1,6,7,9), and PC(1,5,7,8) were respectively used for the enhancement of iron oxide, argillic, phyllic, and propylitic alterations. The eigenvalues are presented in Tables 1 to 4. According to the eigenvalues and the spectral behavior of characteristic bands of alterations, the absolute difference of absorption and reflection values are obtained respectively showing the maximum positive and negative values (shown in red in tables below). Accordingly, the fourth component in tables (1 to 4) was used for the enhancement of iron oxide, argillic, phyllic, and propylitic alterations (Figure 5).

Eigenvector	Band 1	Band 2	Band 3	Band 4
PC1	0.498911	0.505986	0.496898	0.498156
PC2	0.429713	0.2798.5	0.133802	-0.848029
PC3	-0.678828	0.166601	0.692179	-0179794
PC4	**0.325005**	**-0.798706**	0.506042	-0.019001

Table 1. The eigenvalues of correlation for the PC (1,2,3,4) bands.
Source: Based on ASTER data (2020).

Eigenvector	Band 1	Band 5	Band 7	Band 9
PC1	0.484094	0.511759	0.503418	0.500326
PC2	0.867668	-0.382657	-0.202439	-0.244428
PC3	-0.089016	-0.704609	0.110963	0.695190
PC4	0.069868	**0.308549**	**-0.832632**	0.454576

Table 2. The eigenvalues of correlation for the PC (1,5,7,9) bands.
Source: Based on ASTER data (2020).

Eigenvector	Band 1	Band 9	Band 7	Band 9
PC1	0.482707	0.515190	0.502232	0.499336
PC2	0.867866	-0.386556	-0.196845	-0.242149
PC3	-0.094425	-0.711858	0.144024	0.680881
PC4	0.069907	**0.280021**	**-0.829622**	0.477942

Table 3. The eigenvalues of correlation for the PC (1,6,7,9) bands.
Source: Based on ASTER data (2020).

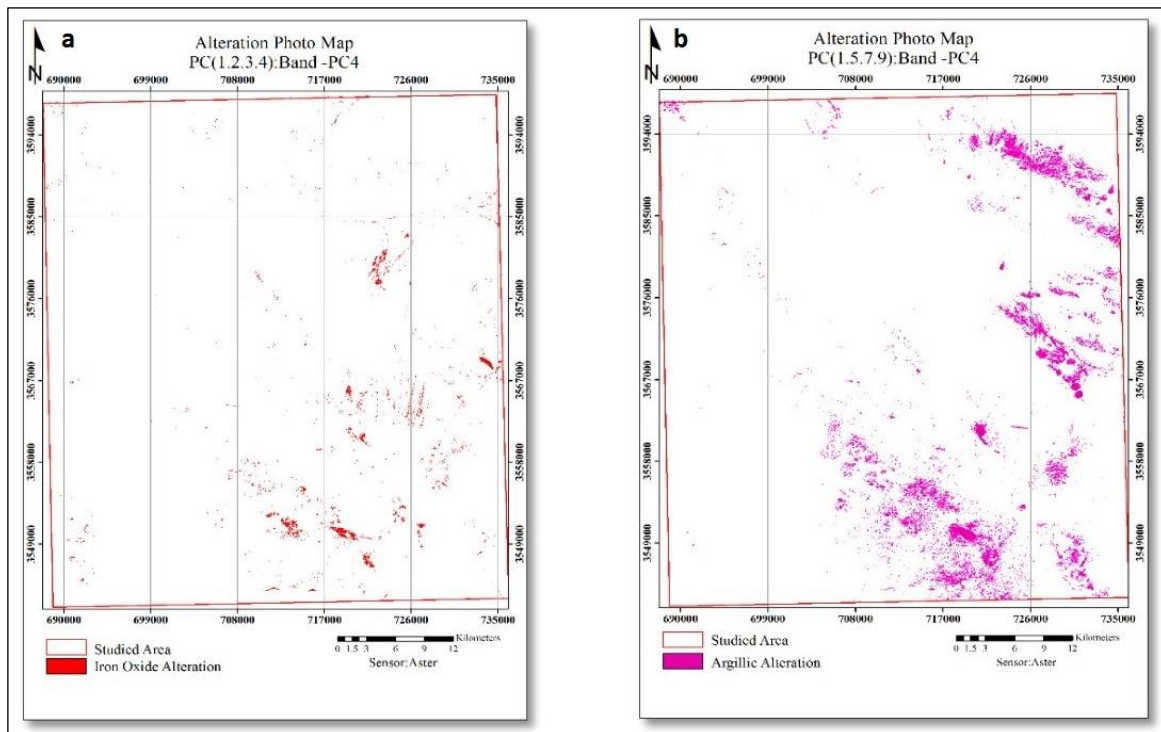Revista Geoaraguaia – **ISSN: 2236-9716** – V.10 n. Especial Geologia e Pedologia. Dez-2020

139

Eigenvector	Band 1	Band 5	Band 7	Table 4: The eigenvalues of correlation for the PC(1,5,7,8) bandsBand 8
PC1	-0.485429	-0.509923	-0.502517	-0.501810
PC2	-0.858343	0.424701	0.241089	0.157327
PC3	0.165567	0.680654	-0.154980	0.296620
PC4	0.0139.2	0.310352	-0.815680	-0.488011

Table 4: The eigenvalues of correlation for the PC(1,5,7,8) bands.
Source: Based on ASTER data (2020).

Revista Geoaraguaia – **ISSN: 2236-9716** – V.10 n. Especial Geologia e Pedologia. Dez-2020
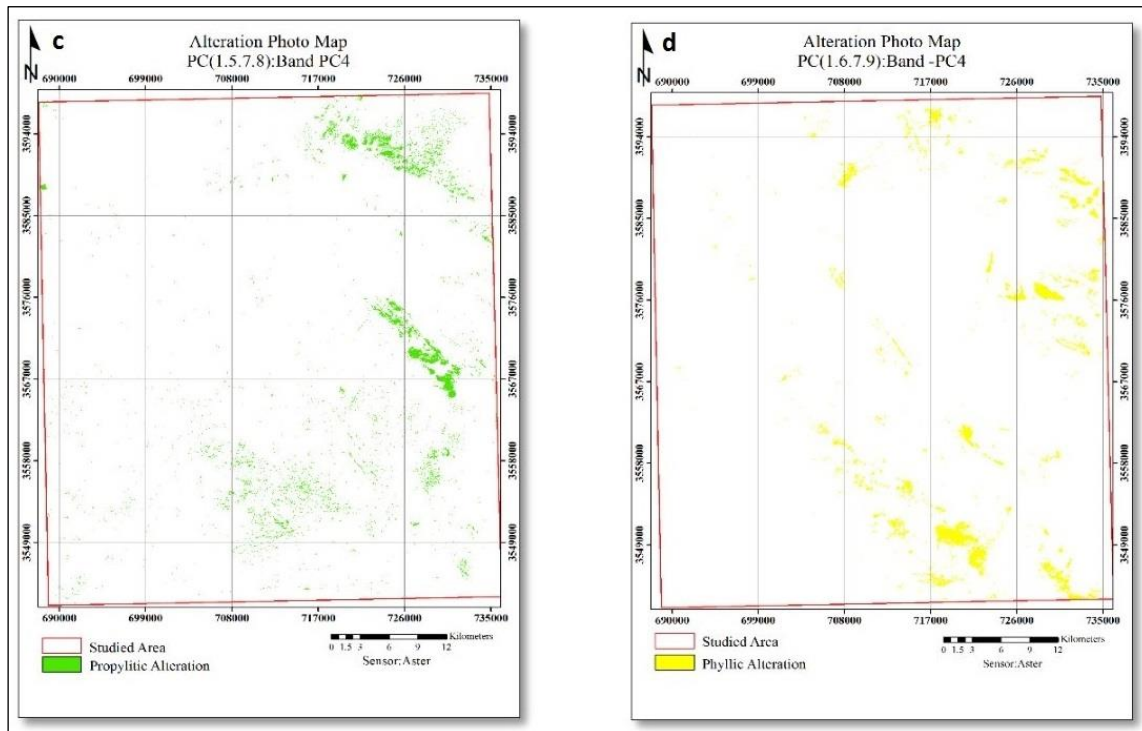
140

Figure 5: Enhancement of alteration distribution by the Crosta method (a: iron oxide, b: argillic, c: phyllic, and d: propylitic). Distribution of iron oxide is more evident in the south to the southeast, the phyllic and argillic alterations in the northeast to the southwest, and the propylitic alteration in the south to the northeast of the sheet.
Source: Based on ASTER data, YAZD STEEL COMPANY (2013).

LS-FIT

LS-Fit is a linear regression between high (absorption) and low (reflection) frequencies, and produces an image of the absorption spectral behavior. The outputs of the algorithm are the residual and prediction images. The prediction image is obtained through predicting other bands, and has the highest similarity with other bands (Yetkin *et al.*, 2004). The residual image shows the prediction error representing the difference of this band with other bands. The residual band can be used to enhnace and extract cetain terrains. In the studied area, the positive, negative, and negative LS-Fit values respectively enhance the band 2 of iron oxide zones, the band 6 of the phyllic and argillic alterations, and the band 8 of the propylitic alteration (Figure 6).
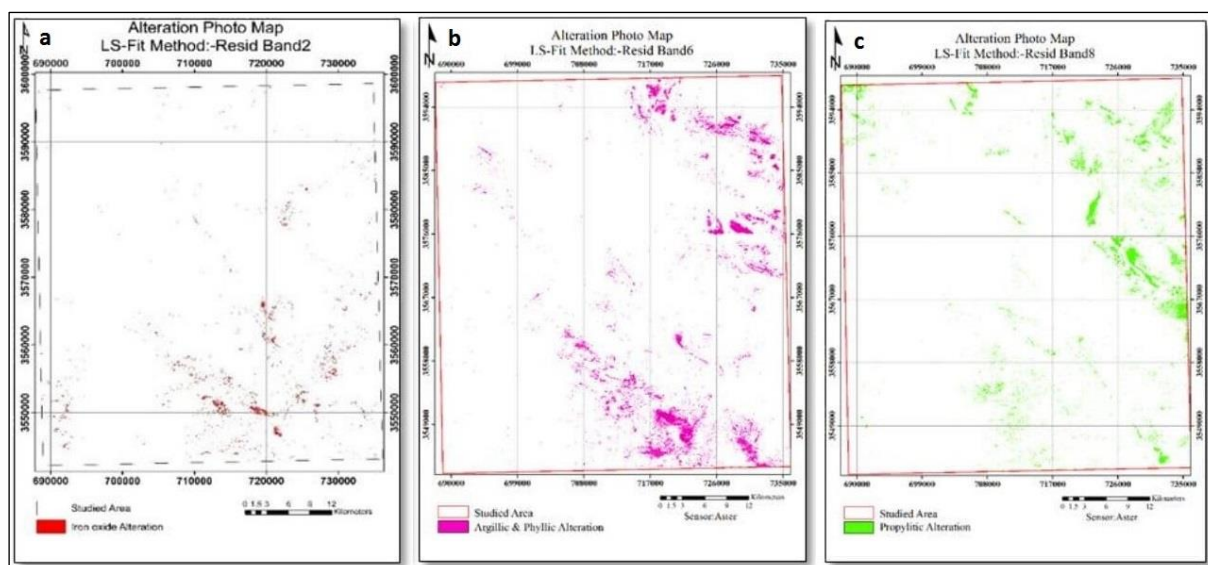
Revista Geoaraguaia – **ISSN: 2236-9716** – V.10 n. Especial Geologia e Pedologia. Dez-2020

141

Figure 6. LS-Fit enhancement of distribution of alterations, (*a*) iron oxide; (*b*) argillic and phyllic; and (*c*) propylitic alterations. Distribution of iron oxide is more evident in the south to the southeast, the phyllic and argillic alterations in the northeast to the southwest, and the propylitic alteration in the south to the northeast of the sheet.
Source: Based on ASTER data, YAZD STEEL COMPANY, 2013.

SPECTRAL ANGLE MAPPER (SAM)

The spectral similarity of the reflectance spectrum of each pixel with that of the reference pixel is used for classification in SAM. This technique is not affected by solar factors, and the angle between two vectors is independent of their lengths (Yektin *et al.*, 2004). This techique provides a qualititative estimation of the simialrity of the spectrum under study with the reference spectrum. In SAM, a brighter pixel corresponds to a larger angle representing the larger difference of the studied spectrum with the reference spectrum. In contrast, a darker pixel is equivalent to a smaller angle representing the higher similarity of both spectra. The spectral behavior of the characteristic minerals in different alterations was used for the enhacement of alterations. The spectral behavior of minerals was compared with that in the USGS spectral library. It was found that all characteristic minerals overlap in the studied alterations (Figure 7).
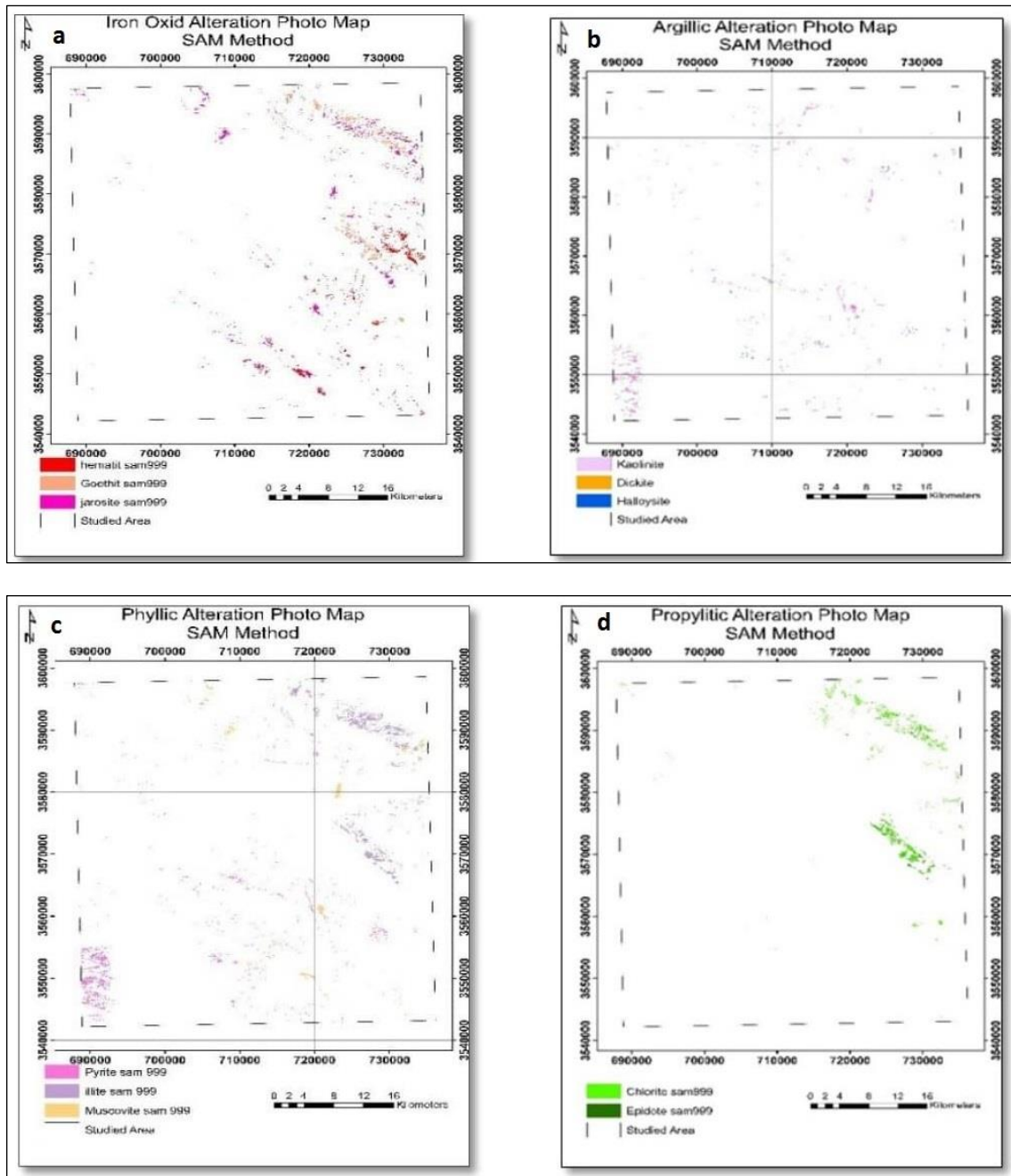
Revista Geoaraguaia – **ISSN: 2236-9716** – V.10 n. Especial Geologia e Pedologia. Dez-2020

142

Figure 7. SAM enhancement of distribution of alterations; (a) iron oxide; (*b*) argillic and phyllic; and (*c*) propylitic. Distribution of iron oxide is more evident in the south to the southeast, the phyllic and argillic alterations in the northeast to the southwest, and the propylitic alteration in the south to the northeast of the sheet.
Source: Based on ASTER data, YAZD STEEL COMPANY, 2013.

SATELLITE IMAGE PROCESSING AND DIGITAL ELEVATION MODEL (DEM)

Revista Geoaraguaia – **ISSN: 2236-9716** – V.10 n. Especial Geologia e Pedologia. Dez-2020

143

The faults and lineaments were determined on the DEM of the study area by relief shading processing (Figure 8). Dehshir–Baft Fault has a north-northwest-south-southeast (NNW-SSE) trend. Sub-faults originated from Dehshir Fault are seen in the west of the fault and the southeast of the sheet on the trachyandesite pyroclastic rocks near Ali Shafi Mountain. Multiple crossed sub-faults parallel to the main fault are observed in the east of the main fault near the Soork iron ore mine. This indicates the undeniable role of Dehshir–Baft Fault mineralization in the Soork iron ore mine. The severe faulting in the southeast of the sheet near Haftar Mountain around the abandoned lead and zinc mines indicates the relationship of mineralization with faulting in this region.
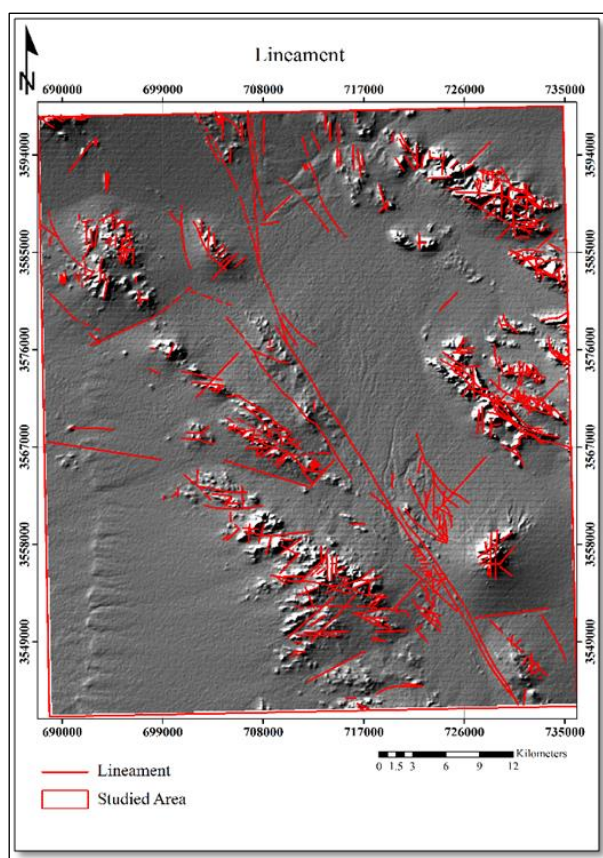

Figure 8. Lineaments of Sarvbala geological sheet. More sub-faults in the south to the southeast of the sheet are affected by the NNW-SSE Dehshir–Baft Fault. Multiple metal mineralizations have occurred along this fault
Source: Shafaii *et al.* (2010)

RESULTS

Revista Geoaraguaia – **ISSN: 2236-9716** – V.10 n. Especial Geologia e Pedologia. Dez-2020

144

INTEGRATION OF INFORMATION LAYERS OF ALTERATIONS AND FAULTS

All alteration layers extracted by different methods were called and integrated in ArcGIS. In the integration process, alterations matched with the geological units were selected as the information layer of alterations. A highest score was given to the mineralization-related units and then integrated with the fault map. The Soork iron deposit in the southeast of the region was used as a useful information layer for integration (Figure 9). A total of 5 rankers were considered in the promising areas for classification of data integration. The promising areas were separated by different colors. As shown in figure 9, there is a good consistency between the information layers in the southeast and southeast of Sarvbala sheet.
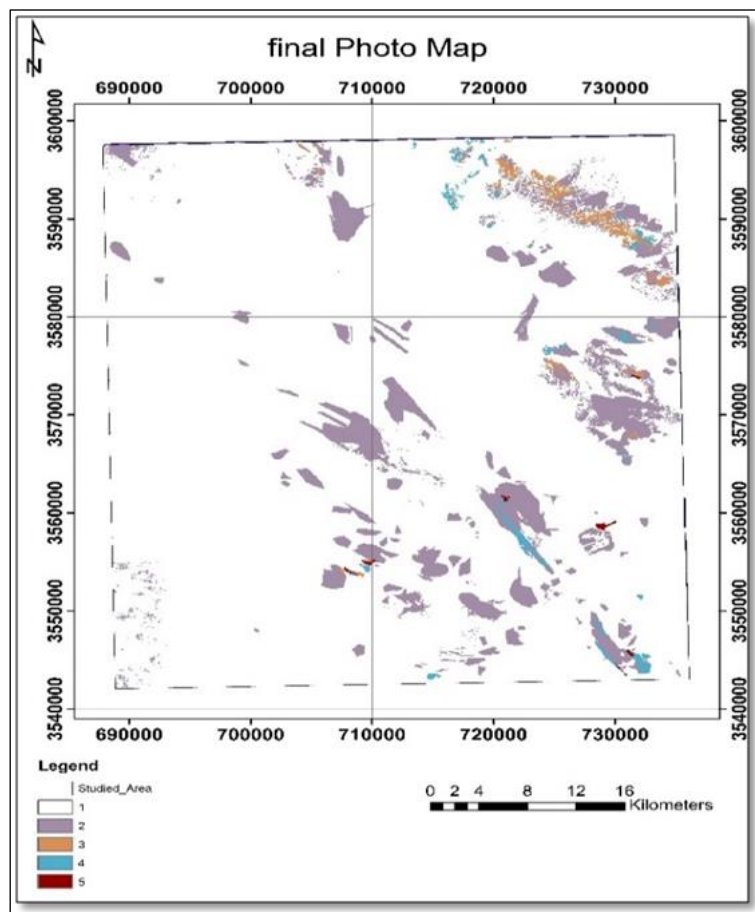

Figure 9. The final map of alterations and faults in Sarvbala geological sheet.
Source: Based on ASTER data, YAZD STEEL COMPANY, 2013

Revista Geoaraguaia – **ISSN: 2236-9716** – V.10 n. Especial Geologia e Pedologia. Dez-2020

145

FIELD OPERATIONS FOR VALIDATION OF ALTERATIONS

After processing of data and preparation of the alteration map, the maps were revised by field operations, and the final map of alterations was prepared (Fig. 10). The enhanced alteration map shows the consistency of the argillic and phyllic alterations confirming field observations (Figure 11).
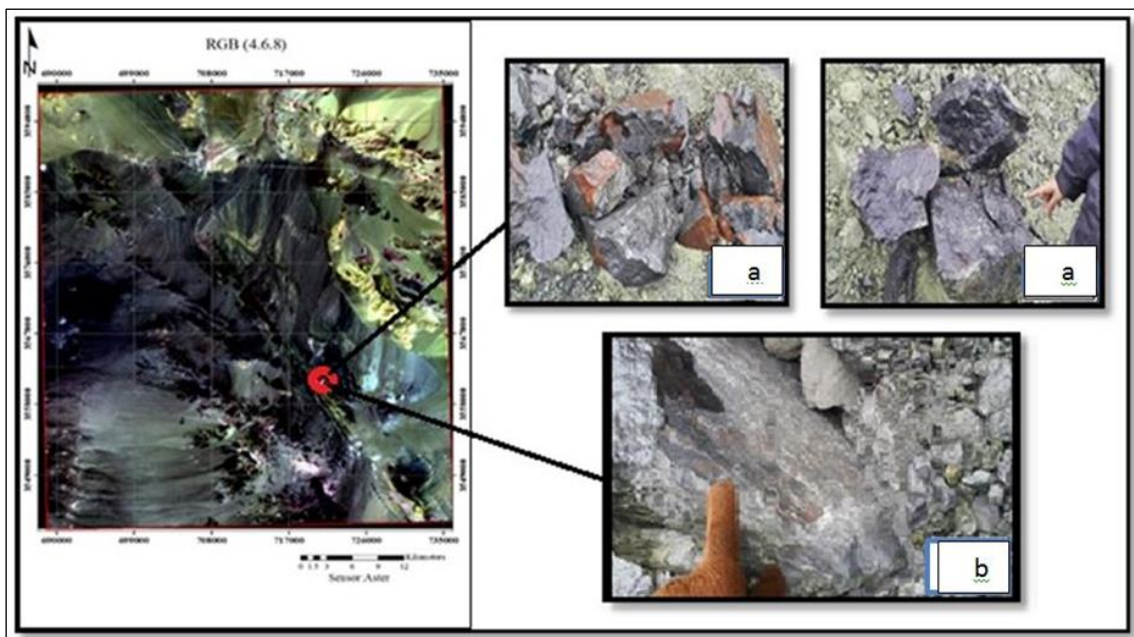

Figure 10. (*a*) The field observation of regions with mineralization and magnetite ore; (*b*) Dehshir–Baft Fault mirror in the mineralization site.
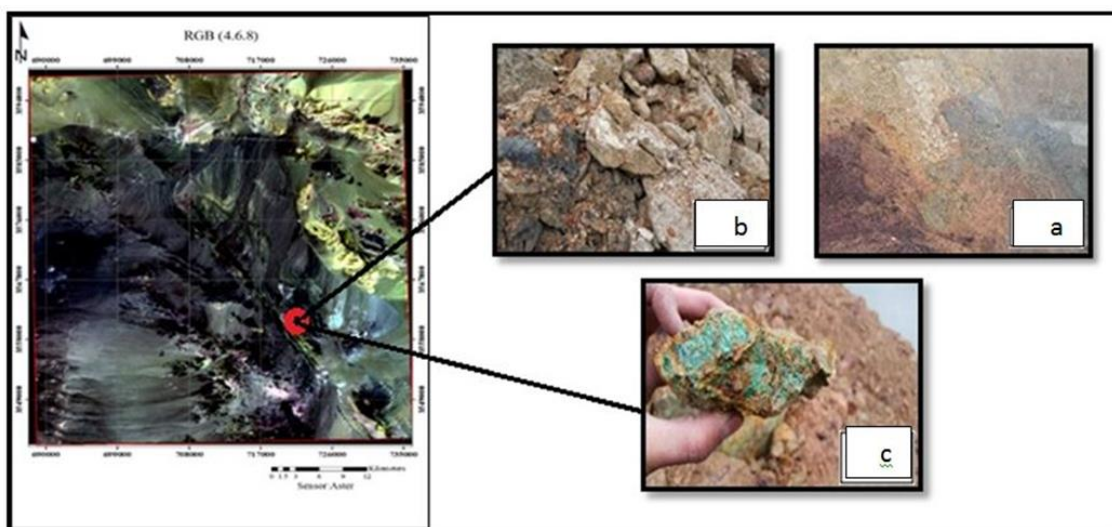Source: YAZD STEEL COMPANY (2013).

Revista Geoaraguaia – **ISSN: 2236-9716** – V.10 n. Especial Geologia e Pedologia. Dez-2020

146

Figure 11. The field observation of regions with (*a*) phyllic alteration; (*b*) argillic alteration; and (*c*) observation of copper and iron ores in Soork.
Source: YAZD STEEL COMPANY (2013).

Field observations confirm the validity of results obtained from remote sensing studies (Figure 7) so that copper and iron indices are seen in some regions. The outcrop of the iron oxide alteration in the vicinity of Dehshir–Baft Fault in Soork (Figure 9) is interestingly consistent with Soork iron deposit in the study area. Figure 10 shows the magnetite ore with hematite. Malachite and azurite are seen with pyrite near the argillic and phyllic alterations in figure 11. The relationship of iron mineralization and related alterations along Dehshir Fault zone was determined respectively after integration of information in ArcGIS (Figure 12).
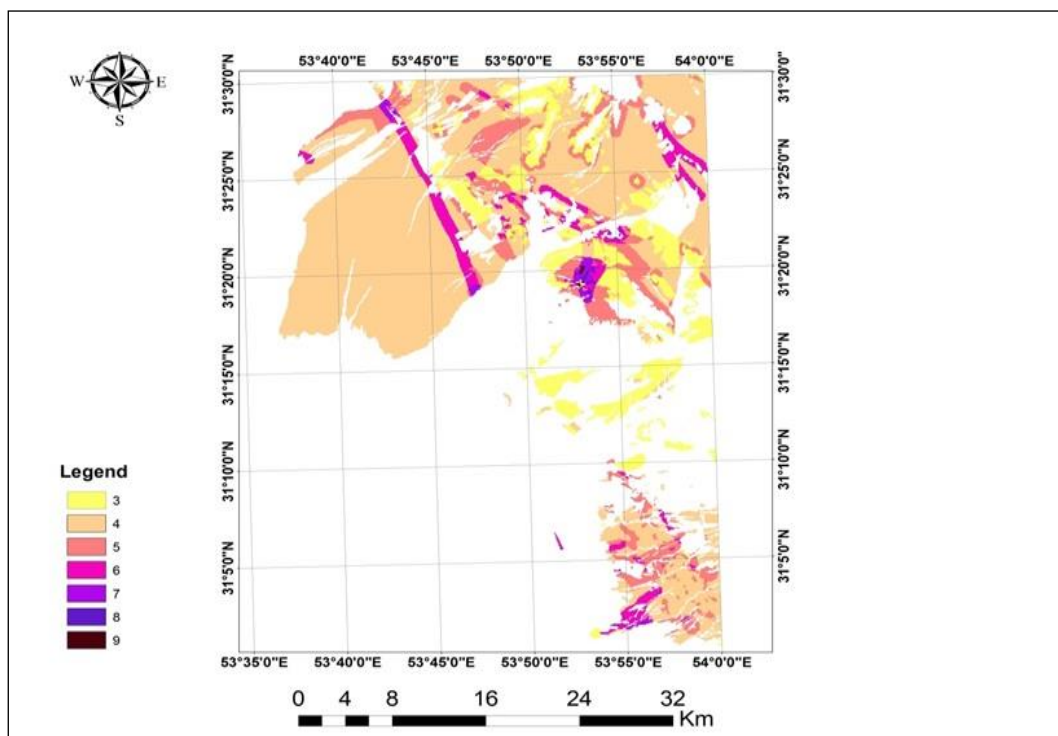

Figure 12. The priority of mineralization exploration in Dehshir sheet.
Source: Based on ASTER data, YAZD STEEL COMPANY (2013).

Revista Geoaraguaia – **ISSN: 2236-9716** – V.10 n. Especial Geologia e Pedologia. Dez-2020

147

THE RELATIONSHIP OF FAULTS AND IRON OXIDE ALTERATIONS IN GIS

The fractal method (Adib *et al.*, 2017) was used to evaluate the relationship of the surface area of iron oxide alteration obtained from the LS-Fit method with their distance from the main Dehshir–Baft Fault. The iron alterations obtained from this method and the main fault in the region were called in ArcGIS and close alterations were converted into a set of close alterations by the command *Merge*. Accordingly, 50 alteration sets and the approximate distance of each iron alteration set with the main Dehshir–Baft Fault were obtained. Table 5 shows the iron alteration layer and the distance and the surface areas of alteration sets. Using data in Table 5, the surface area of iron alterations was calculated, and the fractal diagram (Figure 13) of the logarithm of surface area was plotted against the logarithm of the cumulative frequency of the approximate distance of iron oxide alterations to the main fault (Adib, Mirzaei, 2017). In figure 14, the anti-power of the values obtained from the axis of iron alteration surface areas was classified into 7 categories and then processed in ArcGIS. The final fractal map showing the relationship of the surface areas of iron alterations and their approximate distance from the main Dehshir–Baft Fault was plotted (Afzal, Khakzad, 2010).

Parts	Area(m^2)	Distance(m)	Parts	Area(m^2)	Distance(m)
1	16650	33621	26	145350	500
2	8325	26078	27	8325	400
3	10800	21850	28	22050	2900
4	1800	31145	29	25200	450
5	3150	28575	30	72450	8600
6	43875	25880	31	9000	3200
7	1125	20590	32	225	300
8	35550	13168	33	675	1570
9	44325	3608	34	201375	11600
10	119475	12175	35	31950	6000
11	56475	18090	36	6075	3500
12	99225	15312	37	13950	4600
13	7425	29400	38	1125	2300
14	41850	13900	39	2475	100
15	3600	1798	40	121725	500
16	40050	4976	41	2250	960

Revista Geoaraguaia – **ISSN: 2236-9716** – V.10 n. Especial Geologia e Pedologia. Dez-2020

148

17	107100	1950	42	124200	400
18	13950	750	43	23400	3100
19	82350	2200	44	189450	5300
20	14400	1435	45	225	16000
21	196650	28650	46	548325	11000
22	120375	7900	47	558900	6500
23	14400	800	48	92025	4300
24	66600	150	49	223875	5700
25	4725	90	50	239850	13000

Table 5. The surface area and distance of iron alterations from Dehshir Fault.
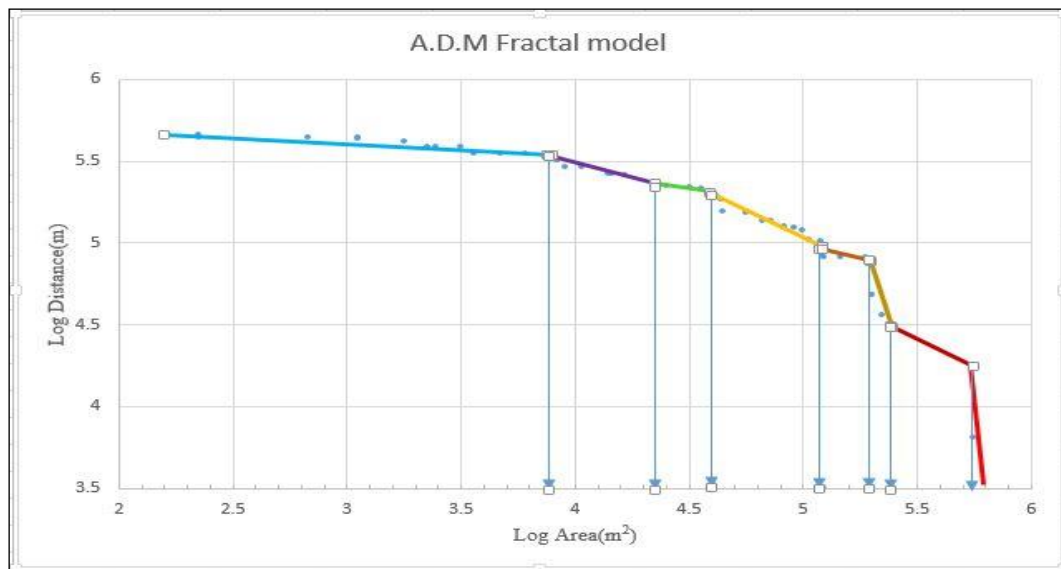Source: Based on ASTER data interpretation (2020).

Figure 13. The fractal diagram of the logarithm of surface area versus the logarithm of the cumulative frequency of the approximate distance of iron oxide alterations from the main fault.
Source: Based on ASTER data interpretation (2020).

Revista Geoaraguaia – **ISSN: 2236-9716** – V.10 n. Especial Geologia e Pedologia. Dez-2020

149
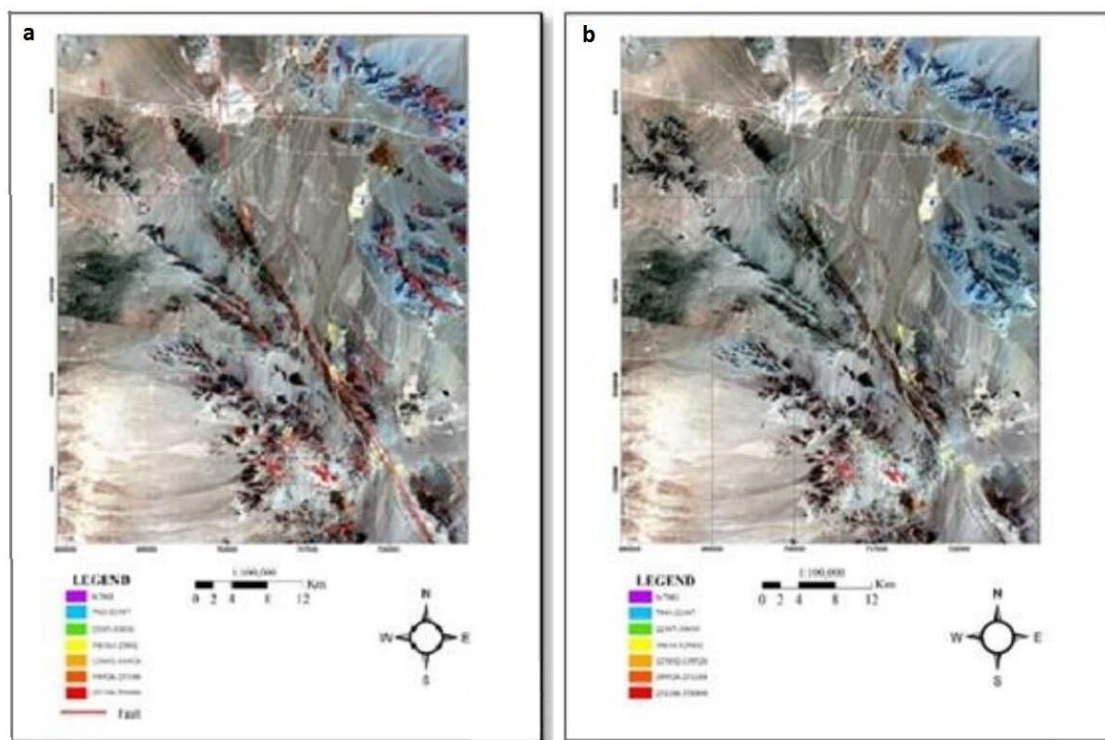
Figure 14. The final fractal map representing the relationship of surface areas of iron alterations and their approximate distance from the main Dehshir–Baft Fault; (*a*) faulting along with separation of the intensity of iron alterations relative to the main fault; (*b*) separation of the intensity of iron alterations relative to the main fault. The relationship of iron alterations with the main faulting is more significant in the southeast of the region. This relationship is more evident in the east of Soork rhyodacite dome and the west of Dehshir–Baft Fault (Soork Fault) indicating a very good consistency with Soork deposit. The red to violet colors show the highest and lowest probable iron anomalies relative to the main fault.
Source: Based on ASTER data, YAZD STEEL COMPANY (2013).

CONCLUSION

Processing of ASTER satellite images using the false color composite (FCC), Crosta, LS-Fit and SAM methods in Envi indicated the maximum concentration of iron oxide, phyllic, argillic, and propylitic alterations in the south to the southeast and in the northeast of the sheet. The information layers of these alterations were integrated with the fault layers, mineralization-related geological units, and existing iron ore deposits, and the results were validated through field observations and operations. The main Dehshir–Baft Fault with north-northwest-south-southeast (NNW-SSE) trend and related sub-faults are seen in the

Revista Geoaraguaia – **ISSN: 2236-9716** – V.10 n. Especial Geologia e Pedologia. Dez-2020

150

east of the main fault near Soork mine. This indicates the undeniable role of Dehshir–Baft Fault mineralization in Soork iron ore mine. The presence of intrusive masses and big Soork and Asmalon iron ore mines respectively in the north and south of Dehshir Fault in Sarvbala and Dehshir sheets is indicative of high mineralization potential of these regions. Given the relationship of iron mineralization in Sarvbala and Khezrabad sheets, this relationship was also explored in Dehshir sheet. After integrating information in ArcGIS, the priority of best regions in Dehshir sheet was determined for detailed study. The fractal method was used to evaluate the relationship of the surface of iron oxide alteration obtained from the LS-Fit method with their distance from Dehshir–Baft Fault. The step fractal curves indicate the multi-phase magnetic field derived from iron mineralization. In other words, a sudden change in the step's slope in the fractal curve may be indicative of a change in the geology, lithology, and mineralization of the region, and also the probable presence of faults, hydrothermal processes, and delayed magma. The structural evaluations and iron oxide alterations indicated the key role of Dehshir–Baft Fault in iron mineralization and the probable presence of porphyritic copper in the depth of south and southeast regions. The presence of abundant faults, alterations existing near Soork Fault (a branch of main Dehshir–Baft Fault), the presence of Soork ore deposit along this fault, and observation of magnetite ores and minerals such as malachite, azurite and alterations related to copper mineralization near Soork and intrusive masses in Tertiary volcanic rocks indicate the likelihood of a large shallow batholith in the study area.

REFERENCES

ABDOLI SERESHGI, H.; GANJI, A.; ASHJA ARDALAN, A.; TORSHIZIAN, H.; TAHERI, J. Detection of metallic prospects using staged factor and fractal analysis in Zouzan region, NE Iran. **Iranian Journal of Earth Sciences**, 11(4), 2019. p. 256-266.

ADIB, A. **Structural analysis and active tectonics of east Yazd**. Ph.D thesis on Structural geology, Islamic Azad University, Science and Research branch, 1998. (In Persian with English abstract).

ADIB, A. Seismic geotechnical microzonation of the Meybod City, **Housing and Urban Development Organization**, Yazd Province, unpublished paper, 2011 (Persian).

Revista Geoaraguaia – **ISSN: 2236-9716** – V.10 n. Especial Geologia e Pedologia. Dez-2020

151

16- Adib, A., Afzal, P., Ilani, S.M., Aliyari, F., 2017. Determination of the relationship between major fault and zinc mineralization using fractal modeling in the Behabad fault zone, central Iran. Journal of African Earth Sciences 134, 308-319

ADIB, A.; MIRZAEI ILANI, S.; SHOAEI, G.; AFZAL, P. Determination of a Conceptual Model for the Structural Features and Pb–Zn   Mineralization in the North of Behabad Fault Zone, Central Iran., **Journal of Earth Sciences,** n.9, 2017. p. 168-183

AFZAL, P.; FADAKAR ALGHALANDIS, Y.; KHAKZAD, A.; MOAREFVAND, P.; RASHIDNEJAD OMRAN, N. Delineation of mineralization zones in porphyry Cu deposits by fractal concentration–volume modeling, **Journal of Geochemical Exploration**, n. 108, 2011. p. 220–232.

AFZAL, P.; FADAKAR ALGHALANDIS, Y.; MOAREFVAND, P.; RASHIDNEJAD OMRAN, N.; ASADI HARONI, H. () Application of power-spectrum-volume fractal method for detecting hypogene, supergene enrichment, leached and barren zones in Kahang Cu porphyry deposit, Central Iran, **Journal of Geochemical Exploration**, n. 112, 2012. p. 131–138.

AFZAL, P.; KHAKZAD, A.; MAAREFVAND, P.; RASHIDNEZHAD, N. A.; FADAKAR, Y. The use of concentration-volume fractal method for separation of zones in porphyry deposits, **Geosciences**, 78, 2010. p. 168-172.

AFZAL, P.; KHAKZAD, A.; MOAREFVAND, P.; RASHIDNEJAD OMRAN, N.; ESFANDIARI, B.; FADAKAR ALGHALANDIS, Y. Geochemical anomaly separation by multifractal modeling in Kahang (Gor Gor) porphyry system, Central Iran, **Journal of Geochemical Exploration**, n. 104, 2010. p. 34–46.

AGHANABATI, A. Geology of Iran. **Iranian Geological Survey and Mineral Exploration Publications**, n. 586, 2004. 640 pp (in Persian).

AGHAZADEH, M.; HOU, Z.; BADRZADEH, Z.; ZHOU, L. Temporal–spatial distribution and tectonic setting of porphyry copper deposits in Iran: Constraints from zircon U–Pb and molybdenite Re–Os geochronology. **Ore Geol. Rev**.70, 2015. p. 385-406.

AHMADI, R.; SHEYKHI, B. Recovery of vanadium from secondary tailing of iron ore by salt roasting-alkaline leaching and solvent extraction processes, **Iranian Journal of Earth Sciences**, 11(1), 2019. p. 30-37.

AMIDI, M.; NABAVI, M. 1:100000 Sarvbala Geological Map, **Geological Survey and Mineral Exploration of Iran**: Tehran, 1980.

DAYA, A. A. Nonlinear disjunctive kriging for the estimating and modeling of a vein copper deposit, **Iranian Journal of Earth Sciences**, 11(3) 2019. p. 226-236.

DEMETS, C.; GORDON, R. G.; ARGUS, D. F.; STEIN, S. Effect Of Recent Revisions To The Geomagnetic Reversal Time Scale On Estimates Of Current Plate Motions. **Geophysical Research Letter**, n. 21, 1994. p. 2191– 2194.

FEIZI, F.; MANSOURI, E. Identification of Alteration Zones with Using ASTER Data in A Part of Qom Province, Central Iran. **Journal of Basic and Applied Scientific Research**, 2(10), 2012. p. 10173-10184.

Revista Geoaraguaia – **ISSN: 2236-9716** – V.10 n. Especial Geologia e Pedologia. Dez-2020

152

FEIZI, F.; MANSOURI, E. Introducing the Iron Potential Zones Using Remote Sensing Studies in South of Qom Province, Iran , **Open Journal of Geology**, n. 3, 2013. p. 278-286.

FEIZI, F.; MANSOURI, E. Separation of Alteration Zones on ASTER Data and Integration with Drainage Geochemical Maps in Soltanieh, Northern Iran. **Open Journal of Geology**, n. 3, 2013. p. 134-142.

MANSOURI, E .; FEIZI, F., KARBALAEI RAMAZANALI, A. A. Recognition of a porphyry system using remote sening in Bideghan – Qom provice, **Journal of Basic Sciences,** n.6, 2012. p. 73-84.

MIRZAEE, S. **The Study of Relation of Structural Features with Mineralization of the Behabad Area**. MSc Thesis on Structural geology, Islamic Azad University, North Tehran Branch, 2012. (in Persian with English abstract).

NAZARPOUR, A. Application of C-A fractal model and exploratory data analysis (EDA) to delineate geochemical anomalies in the: Takab 1:25,000 geochemical sheet, NW Iran, **Iranian Journal of Earth Sciences**, 10(2), 2018. p. 173-180.

NAZEMI, E.; ARIAN, M.A.; JAFARIAN, A.; POURKERMANI, M.; YAZDI, A. Studying The Genesis Of Igneous Rocks In Zarin-Kamar Region (Shahrood, Northeastern Iran) By Rare Earth Elements, **Revista Gênero e Direito**, 8(4), 2019. p. 446-466. DOI: <https://doi.org/10.22478/ufpb.2179-7137.2019v8n4.48442>

NOURI, R.; JAFARI, M. R.; ARAIN, M.; FEIZI, F. Hydrothermal Alteration Zones Identification Based on Remote Sensing Data in the Mahin Area, West of Qazvin Provice, Iran, Proceeding of World Academy of Science, Engineering and Technology, **World Academy of Science, Engineering and Technology**, n. 67, 382-385, 2012.

NOVRUZOV, N.; VALIYEV, A.; BAYRAMOV, A.; MAMMADOV, S.; IBRAHIMOV, J.; EBDULREHIMLI, A. Mineral composition and paragenesis of altered and mineralized zones in the Gadir low sulfidation epithermal deposit (Lesser Caucasus, Azerbaijan), **Iranian Journal of Earth Sciences**, 11(1), 2019. p. 14-29.

RASI, R.; AFZAL, P. Separation of anomaly communities of gold-bearing veins in Sharafabad–Hizejan (East Azerbaijan) by the concentration-number fractal method., **33rd National Conference on Geosciences, Geological Survey and Mineral Exploration of Iran**, 2014.

SHAFAII MOGHADAM, H.; J.STERN, R.; RAHGOSHAY, M. The Dehshir ophiolite (central Iran): Geochemical constraints on the origin and evolution of the Inner Zagros ophiolite belt. GSA **Bulletin,** 122 (9-10), , 2010. p. 1516–1547.

STOCKLINE, J.; EFTEKHRNEJAD, J.; HOSHMANDZADEH, A. Geology of the Shotori Range. **Geological Survey of Iran**, n. 3, 1968. p. 69.

TOOSI, H. **Introduction of a porphyry system using remote sensing techniques in Hasankuh in 1:100000 Farmahin sheet**, MSc thesis, Islamic Azad University, South Tehran Branch, 2015.

ULRICH, T.; GUNTHER, D.; HEINRICH, C. A. The evolution of a porphyry Cu_Au deposite, based on La-ICP-MS analysis of fluid inclusions, Bajo de la Alumbera, Argentina, **Economic Geology**, n. 96, 2001. p. 1743-1774.

Revista Geoaraguaia – **ISSN: 2236-9716** – V.10 n. Especial Geologia e Pedologia. Dez-2020

153

WALKER, R. T.; JACKSON, J. Offset and Evolution of the Gowk Fault, S.E. Iran:A Major Intra-Continental Strike-Slip System, **Journal of Structural Geology**, n. 24, 2002. p. 1677–1698.

WALKER, R. T.; TALEBIAN, M.; SAIFFORI, S.; SLOANM R. A.; RASHEEDI, A.; MAC BEAN, N.; GHASSEMI, A. () Active Faulting, Earthquakes, and Restraining Bend Development near Kerman City in Southeastern Iran: **Journal of Structural Geology**, n. 32, 2010. p. 1046–1060.

YASREBI, A. B.; HEZARKHANI, A. Resources classification using fractal modelling in Eastern Kahang Cu-Mo porphyry deposit, Central Iran, **Iranian Journal of Earth Sciences**, 11(1), 2019. p. 56-67.

YAZD STEEL COMPANY, **Exploration Operation during Extraction of Soork Iron Ore Mine (Sadat 2)**. Industry Mine and Trade Organization: Yazd Province, 2013.

YAZDI, A.; ASHJA-ARDALAN, A.; EMAMI, M. H.; DABIRI, R.; FOUDAZI, M. Magmatic interactions as recorded in plagioclase phenocrysts of quaternary volcanics in SE Bam (SE Iran), **Iranian Journal of Earth Sciences**, 11(3), 2019a. p. 215-224.

YAZDI, A.; ASHJA-ARDALAN, A.; EMAMI, M. H.; DABIRI, R.; FOUDAZI, M. Chemistry of Minerals and Geothermobarometry of Volcanic Rocks in the Region Located in Southeast of Bam, Kerman Province. **Open Journal of Geology**, n. 7, 2017. p. 1644-1653. DOI: <10.4236/ojg.2017.711110>

YAZDI, A.; SHAHHOSINI, E.; DABIRI, R.; ABEDZADEH, H. Magmatic Differentiation Evidences And Source Characteristics Using Mineral Chemistry In The Torud Intrusion (Northern Iran), **Revista GeoAraguaia**, 9(2), 2019b. p. 6-21.

YETKIN, E.; TOPRAK, V.; SUEZEN, M. L. Alteration Mapping By Remote Sensing: Application to Hasandag-Melendiz Volcanic, Complex. Geo-Imagery Bridging Continents **XXth ISPRS Congress**, Istanbul, 2004.

ZADMEHR, F.; SHAHROKHI, S. V. Separation of geochemical anomalies by concentration-area and concentration-number methods in the Saqez 1:100,000 sheet, Kurdistan, **Iranian Journal of Earth Sciences**, 11(3), 2019. p. 196-204.

ZAMYAD, M.; AFZAL, P.; POURKERMANI, M.; NOURI, R.; JAFARI, M. R. Determination of Hydrothermal Alteration Zones Using Remote Sensing Methods in Tirka Area, Toroud, NE Iran., **Journal of the Indian Society of Remote Sensing**, n.47 2019. p. 1817–1830 DOI:<10.1007/s12524-019-01032-3>

Revista Geoaraguaia – **ISSN: 2236-9716** – V.10 n. Especial Geologia e Pedologia. Dez-2020

154